Journal of
Materials in Life Sciences

Vol. 5 No. 1 (2026)

Full Paper

Structural and Optical Characterisation of Sb_2MoO_6 Flower-Like Microstructures

Nurul Izzati Muhammad Afdhal[a], Muhammad Izzudin Mohamad[a], Nurrulhidayah Salamun[a], Nursyafreena Attan[a], Siti Aminah Setu[a], Fuad Mohamad[a,*]

[a] Department of Chemistry, Faculty of Science, Universiti Teknologi Malaysia, 81310 UTM Johor Bahru, Johor, Malaysia.

Article history
Received
9 March 2026
Revised
11 April 2026
Accepted
29 April 2026
Published online
30 May 2026

*Corresponding author
m.fuad@utm.my

Abstract

A comprehensive structural and optical characterisation was conducted on antimony molybdate (Sb_2MoO_6) flower-like microstructures to assess their structural and electronic properties. X-ray diffraction and Raman spectroscopy confirmed a crystalline composite framework, mainly comprising Sb_2O_4 and MoO_2 phases. Field emission scanning electron microscopy showed a unique 3D flower-like morphology composed of self-assembled nanosheets that formed porous microspheres with an average diameter of 4.19 ± 0.81 µm. X-ray photoelectron spectroscopy verified the oxidation states of Sb^{3+} and $Mo^{6+,}$ confirming the presence of Sb and Mo in the metal oxide composite. Optical studies with UV-Visible diffuse reflectance spectroscopy identified a direct band gap of 2.48 eV. These findings indicate that the microwave-assisted synthesis produces hierarchical structures with electronic properties suited for advanced functional applications.

Keywords : Microwave-assisted hydrothermal, Hierarchical architecture, Flower-like microspheres, Optical band gap, Molybdates, Sb_2MoO_6

© 2026 Penerbit UTM Press. All rights reserved

1.0 INTRODUCTION

Transition metal molybdates with the general formulas $MMoO_4$ and M_2MoO_4 (M = transition metal) have garnered a significant attention recently.[1], [2], [3] They have distinct crystal structures and tunable electronic properties which make them promising candidates for a variety of functional applications.[4], [5] The presence of multiple oxidation states in transition metals enables the synthesis of various nanostructures which include hierarchical structures like Sb_2MoO_6, $CoMoO_4$ and $NiMoO_4$, as well as their hybrids with carbon-based materials for enhanced electrochemical performance.[1], [6]

Among these, Sb_2MoO_6 has emerged as a particularly interesting metal oxide due to the synergistic interaction between Sb^{3+} and Mo^{6+} species.[1], [5], [7] Molybdenum-based compounds exhibit rich redox chemistry (Mo^{6+}/Mo^0), suitable working potentials, and stable three-dimensional frameworks, which contribute to good charge-discharge cycling and efficient ion transport, making them attractive for energy storage and catalysis.[2], [6] Structurally, MoO_6 octahedra can form layered or tunnel configurations through various connectivity modes, further enhancing their functional versatility.[6] In Sb_2MoO_6, the presence of Sb^{3+} lone-pair electrons coupled with MoO_6 octahedral units introduces a synergistic effect that enhances chemical reactivity and light-harvesting capability.[4], [8] The morphology and hierarchical structure of Sb_2MoO_6 have a significant influence on its performance.[7], [9]

Traditional methods such as hydrothermal and solid-state synthesis techniques frequently produce materials with poorly defined morphologies and small surface areas, which limit the accessibility of active sites.[1], [8] To address these limitations, 3D hierarchical architectures, particularly flower-like microspheres assembled from two-dimensional nanosheets,

have been developed to enhance porosity, mass transport, and light–matter interaction.[4], [7] Microwave-assisted hydrothermal synthesis offers a powerful alternative, providing rapid and uniform heating. This method improves the crystallinity and provides precise morphological control within reduced reaction times.[7], [9] Despite growing interest, a comprehensive understanding of the physicochemical and optical properties of microwave-synthesised Sb_2MoO_6 remains limited.

In this study, hierarchical Sb_2MoO_6 flower-like microspheres were synthesised *via* a rapid 90-minute microwave-assisted hydrothermal method. The material was characterised in terms of structure, vibrational properties, morphology, and optical behaviour. This work establishes a clear structure–property relationship, highlighting the potential of Sb_2MoO_6 as a high-performance material for photocatalytic and electrochemical applications.

2.0 EXPERIMENTAL

2.1 Microwave-Assisted Hydrothermal Synthesis of Sb_2MoO_6

Antimony (III) trichloride ($SbCl_3$, 99.95%), sodium molybdate (VI) dihydrate ($Na_2MoO_4.2H2O$, 99%), and ethanol (98%) were purchased from Sigma-Aldrich and used as received without further purification. Deionised (DI) water was used throughout the synthesis and cleaning processes. The Sb_2MoO_6 flower-like microspheres were synthesized using a modified one-step microwave-assisted hydrothermal route as reported by Lu *et al*. (2019).[7] $SbCl_3$ (0.19 g) and of $Na_2MoO_4.2H_2O$ (0.10 g) were dissolved in 30 mL of DI water. The solution was stirred vigorously until a homogenous precursor was formed. The mixture was transferred to a 50 mL Teflon-lined microwave digestion vessel and heated in a microwave system at 160˚C for 90 minutes. After cooling to room temperature, the resulting green precipitate was collected *via* centrifugation (6000 rpm), washed multiple times with DI water and ethanol to remove residual ions, and dried in a vacuum oven at 60˚C for 12 hours.

2.2 Structural, Chemical and Optical Characterisation Sb_2MoO_6

The crystal phase was determined using X-ray diffraction (XRD, Rigaku SmartLab) with Cu-Kα radiation (λ = 1.3923 Å) in the 2θ range of 3˚ to 100˚. Raman spectra were recorded using a 633 nm laser source to identify the metal-oxide bonding modes. X-ray photoelectron spectroscopy (XPS) was used to determine elemental oxidation states. Morphological evaluation and elemental mapping were carried out using field emission scanning electron microscopy (FESEM) and energy dispersive X-ray (EDX) spectroscopy at an accelerating voltage of 20 kV. The average diameter and size distribution of the Sb_2MoO_6 microspheres were determined by statistical analysis of the FESEM micrographs using ImageJ software. The band gap energy was determined using UV-Visible Diffuse Reflectance Spectroscopy (UV-DRS, Shimadzu UV-2600). The direct band gap was estimated using the resulting Tauc plot.

3.0 RESULTS AND DISCUSSION

3.1 Phase and Vibrational Analysis (XRD and Raman)

The crystalline phase of the synthesised Sb_2MoO_6 was investigated using XRD. The diffraction pattern reveals a monoclinic crystal system ($\alpha = \gamma = 90^{\circ}$, $\beta \neq 90^{\circ}$, a = 5.60 Å, b = 4.85 Å and c = 5.61Å) with most intense peak recorded at $2\theta = 28.47^{\circ}$ (see Figure 1a). The diffraction pattern is consistent with standard JCPDS data (No. 33-1491) and previously reported studies[1], [7], [8], [9], confirming the formation of the expected phase of Sb_2MoO_6. However, while earlier works reported a triclinic structure, the present study observed a monoclinic crystal system. The sharp peaks indicating that the microwave-assisted hydrothermal process successfully promoted high crystallinity. Further analysis identifies a nanocrystalline composite primarily composed of Sb_2O_4 (~91%) and MoO_2 (~9%) phases with an average crystallite size of 1.83 nm. Raman spectroscopy was used to investigate the vibrational modes of the metal-oxide Sb_2MoO_6 framework. For Mo-O Raman bands, a prominent stretching mode at 768 cm^{-1} correspons to the Mo-O-Mo symmetric stretching, 885 cm^{-1} is assigned to the terminal Mo=O bond stretching and the peak at 696 cm^{-1} is attributed to the asymmetric stretching of the Mo–O–Mo of the MoO_6 octahedra (see Figure 1b).[5], [10], [11] Importantly, the incorporation of Sb into the oxide lattice is verified by the peaks at 331 cm^{-1} and 480 cm^{-1}.[12] The former refers to Sb–O bending vibrations, while the latter corresponds to the Sb–O–Sb stretching mode. The alignment between XRD and Raman data confirms the formation of a long-range ordered lattice despite the short synthesis duration.

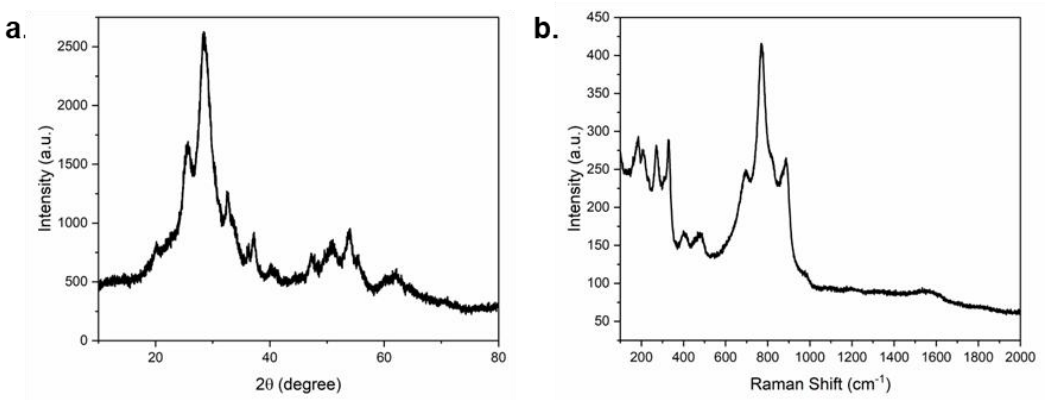


Figure 1 : (a) XRD pattern showing 2θ peaks at 25.61˚, 28.47˚, 36.13˚, 37.23˚, 51.08˚, 53.75 and 61.41˚; and (b) Raman spectrum of Sb_2MoO_6 showing most intense Raman shift at 768 cm^{-1}.

3.2 Morphology and Composition Analysis (FESEM-EDX)

Following the method reported by Lu *et al*. (2019), hierarchical Sb_2MoO_6 microstructures were successfully synthesised. The surface morphology of Sb_2MoO_6 was examined using FESEM while the elemental composition was obtained from the EDX analysis. The previous study by Lu *et al*. (2019) described microspheres formed from 1D nanobelts,[7] however the current results show a 3D flower-like morphology composed of interconnected 2D sheets with significant surface due to the porosity and hierarchical structures. (see Figure 2). The microspheres had an average diameter of 4.19 ± 0.81 µm. This variation in hierarchical assembly is probably due to the local kinetic factors and thermal distribution within the microwave cavity.

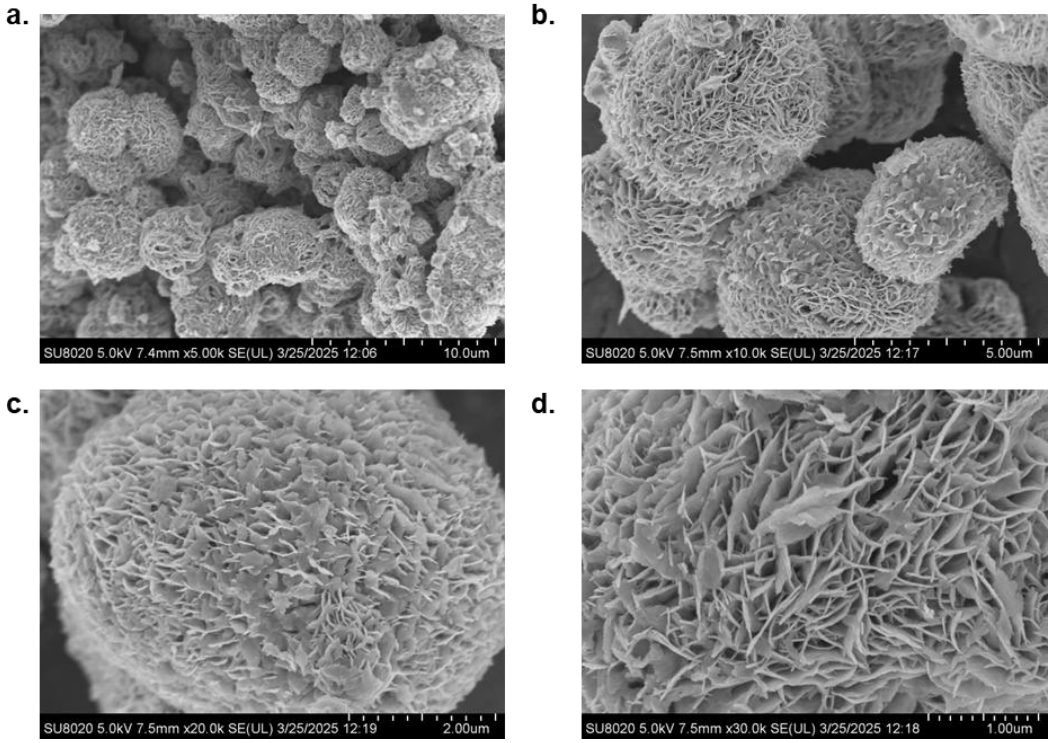


Figure 2 : The FESEM images of the as prepared 3D flower-like morphology composed of interconnected 2D sheets at magnifications at (a) 5,000, (b) 10,000, (c) 20,000 and (d) 30,000.

The elemental composition of the flower-like microspheres was determined using EDX analysis. Table 1 summarises the outcomes of two studies, as well as the theoretical and literature values. The atomic percentages for Trial 1 (Sb: 24.37%, Mo: 9.09%, O: 66.53%) are consistent with the theoretical stoichiometry of Sb_2MoO_6 (2:1:6 ratio) and the values reported by Lu et al. (2019). However, Trial 2 has a higher Sb content (28.17%), resulting in an Sb-rich stoichiometry that approximates 3:1:7, probably due to the localised composition variation within the sample.

Table 1: Atomic Percent (%) of Sb, Mo and O from EDX Analysis of Sb_2MoO_6

Element	Atomic Percent (%)			
	Trial 1	Trial 2	Theoretical	Lu et al. (2019)[7]
Sb	24.37	28.17	22.22	22.87
Mo	9.099	8.74	11.11	11.07
O	66.53	63.09	66.67	66.86
Ratio Sb:Mo:O	2:1:6	3:1:7	2:1:6	2:1:6

3.3 Surface Chemistry Analysis (XPS)

The surface chemical composition and oxidation states of the Sb_2MoO_6 hierarchical microspheres were studies using XPS analysis. The survey spectrum indicates the presence of Sb, Mo, and O, which is consistent with the EDX results (see Figure 3a). The high-resolution spectrum of Sb 3d displays two major peaks located at around 530 eV ($3d_{5/2}$) and 540 eV ($3d_{3/2}$) (see Figure 3b). The peak positions and separation of ~10 eV indicate the Sb^{3+} oxidation state within an oxide lattice.[13], [14] Note that also the peak of Sb $3d_{5/2}$ (~530 eV) typically overlaps with the O 1s peak, thus contributing to its high intensity. The high-resolution Mo 3d spectrum exhibits two distinct peaks at ~233 eV ($3d_{5/2}$) and 236 eV ($3d_{3/2}$) (see Figure 3c). These peak positions and the binding energy peak separation of 3 eV confirm the presence of Mo in the Mo^{6+} oxidation state. The synthesis of high purity Sb_2MoO_6 with the expected electrical configurations is clearly demonstrated by these XPS results, which are in line with the previous published research.[1], [8], [14]

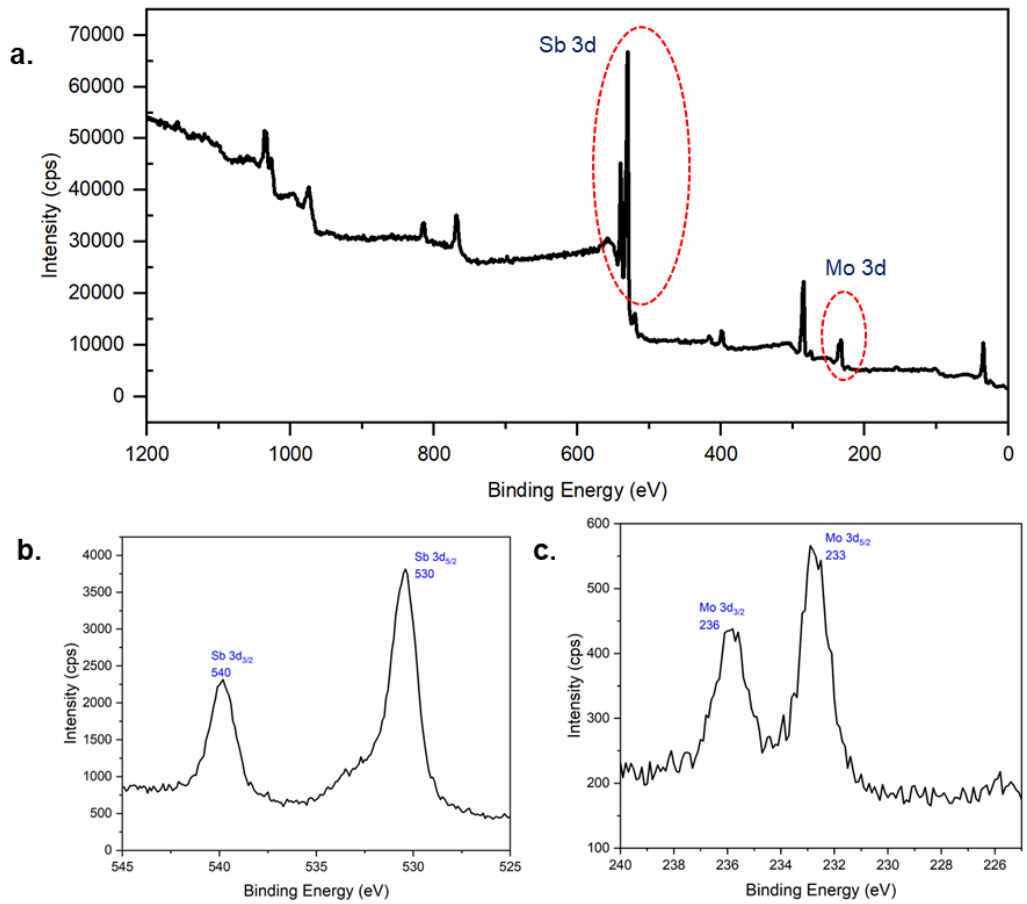


Figure 3 : XPS spectra of the hierarchical Sb_2MoO_6 flower-like microspheres: (a) wide survey scan indicating the elemental constituents; (b) high-resolution core-level spectrum of Sb 3d; and (c) high-resolution core-level spectrum of Mo 3d.

3.4 Optical Properties (UV-DRS)

UV-DRS was used to analyse the optical properties of Sb_2MoO_6. The reflectance spectrum of the hierarchical Sb_2MoO_6 microspheres exhibits two distinct optical regimes: (I) 200 – 420 nm and (II) >420 nm (see Figure 4a). In the UV and visible region (up to ~420 nm), the reflectance is at its minimum, indicating maximum absorbance as photons possess sufficient energy to overcome the energy gap. Conversely, for wavelengths beyond 420 nm, a sharp increase in reflectance is observed, suggesting that the material becomes poorly absorbing in the longer wavelength visible region. This steep transition corresponds to the estimated direct band gap of 2.48 eV based on the Tauc plot (see Figure 4b).

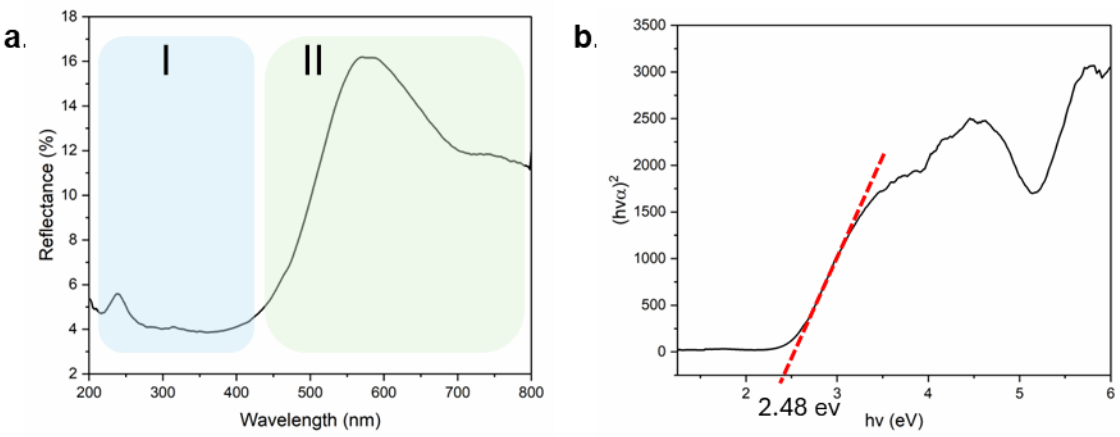


Figure 4: (a) Reflectance spectrum and (b) Tauc plot of Sb_2MoO_6.

4.0 CONCLUSION

Sb_2MoO_6 flower-like microstructures were successfully synthesised using microwave-assisted hydrothermal method and were physico-chemically characterised. The XRD pattern exhibited sharp diffraction peaks indicating high crystallinity with most intense peak recorded at 2θ = 28.47˚. Raman spectroscopy analysis showed characteristic Mo-O (696, 768 and 885 cm^{-1}) and Sb-O (331 and 480 cm^{-1}) vibrational modes, confirming the incorporation of Sb into the crystal lattice and the formation of Sb_2MoO_6. FESEM morphological analysis demonstrated the formation of 3D flower-like microspheres with assembled from interconnected 2D nanosheets, with increased surface area and porosity. This observation differs from previously described nanobelt-based morphologies. The average size of the microspheres is estimated around 4.19 ± 0.81 µm. XPS investigation verified the existence of Sb^{3+} and Mo^{6+} oxidation states which is consistent with the EDX results. UV-DRS investigation showed minimum reflectance thus high absorption up to ~420 nm, with a direct band gap of 2.48 eV, indicating suitable for visible-light applications.

Acknowledgment

The authors would like to acknowledge all individuals who have supported this research, especially the Department of Chemistry, Faculty of Science, Universiti Teknologi Malaysia, for providing laboratory facilities and technical assistance. The authors gratefully acknowledge *Geran Penyelidikan* Hi-Tech(F4) (Ref. No.: PY/2022/04804, Cost Centre No.: Q.J130000.4654.00Q25) and Potential Academic Staff Grant - DTD Fund (PAS DTD) (Ref. No.: PY/2024/02212, Cost Centre No.: R.J130000.8054.4J723).

References

[1] R. Li, H. Yue, R. Jin, and S. Chen, 'Hierarchical Sb2MoO6 hollow spheres modified with carbon nanotubes and amorphous carbon for enhance lithium ion storage', *Solid State Ion.*, vol. 363, May 2021, doi: 10.1016/j.ssi.2021.115587.
[2] X. Ge *et al.*, 'High-specific-capacity molybdate anode materials for lithium-ion batteries with good low-temperature performance', *J. Alloys Compd.*, vol. 903, May 2022, doi: 10.1016/j.jallcom.2022.163914.
[3] A. Rehman, S. Saleem, S. Ali, S. M. Abbas, M. Choi, and W. Choi, 'Recent advances in alloying anode materials for sodium-ion batteries: material design and prospects', *Energy Materials*, vol. 4, no. 6, Jul. 2024, doi: 10.20517/energymater.2024.06.
[4] S. Yuan *et al.*, 'Self-Assembled 3D Hierarchical Porous Bi2MoO6 Microspheres toward High Capacity and Ultra-Long-Life Anode Material for Li-Ion Batteries', *ACS Appl. Mater. Interfaces*, vol. 9, no. 26, pp. 21781–21790, Jul. 2017, doi: 10.1021/acsami.7b04045.
[5] J. Wang *et al.*, 'Nature of Bimetallic Oxide Sb2MoO6/rGO Anode for High-Performance Potassium-Ion Batteries', *Advanced Science*, vol. 6, no. 17, Sep. 2019, doi: 10.1002/advs.201900904.

[6] J. Xie, H. Zhang, Q. Liu, X. Liu, and X. Lu, 'Recent progress of molybdenum-based materials in aqueous rechargeable batteries', Dec. 01, 2020, *Elsevier Ltd*. doi: 10.1016/j.mtadv.2020.100100.
[7] X. Lu *et al.*, 'Hierarchical Sb2MoO6 microspheres for high-performance sodium-ion battery anode', *Energy Storage Mater.*, vol. 17, pp. 101–110, Feb. 2019, doi: 10.1016/j.ensm.2018.11.021.
[8] Y. Zhao, H. Shi, D. Yang, J. Fan, X. Hu, and E. Liu, 'Fabrication of a Sb2MoO6/g-C3N4Photocatalyst for Enhanced RhB Degradation and H2Generation', *Journal of Physical Chemistry C*, vol. 124, no. 25, pp. 13771–13778, Jun. 2020, doi: 10.1021/acs.jpcc.0c03209.
[9] X. Lu *et al.*, 'Enabling high-performance sodium metal anodes via A sodiophilic structure constructed by hierarchical Sb2MoO6 microspheres', *Nano Energy*, vol. 69, Mar. 2020, doi: 10.1016/j.nanoen.2020.104446.
[10] W. T. Chen *et al.*, 'Porous nitrogen-doped carbon supported MoO2/Mo2C hybrid catalyst for efficient oxidative coupling of primary amines to imines', *Journal of Porous Materials*, vol. 30, no. 3, pp. 705–712, Jun. 2023, doi: 10.1007/s10934-022-01375-2.
[11] R. L. Frost, J. Bouzaid, and I. S. Butler, 'Raman spectroscopic study of the molybdate mineral Szenicsite and comparison with other paragenetically related molybdate minerals', *Spectroscopy Letters*, vol. 40, no. 4, pp. 603–614, Jul. 2007, doi: 10.1080/00387010701301220.
[12] S. Bahfenne and R. L. Frost, 'Raman spectroscopic study of the antimony bearing mineral langbanite', *Spectrochim. Acta A Mol. Biomol. Spectrosc.*, vol. 75, no. 2, pp. 710–712, Feb. 2010, doi: 10.1016/j.saa.2009.11.043.
[13] M. Hu, Y. Jiang, W. Sun, H. Wang, C. Jin, and M. Yan, 'Reversible conversion-alloying of Sb2O3 as a high-capacity, high-rate, and durable anode for sodium ion batteries', *ACS Appl. Mater. Interfaces*, vol. 6, no. 21, pp. 19449–19455, Nov. 2014, doi: 10.1021/am505505m.
[14] A. G. Nguyen, H. T. T. Le, R. Verma, D. L. Vu, and C. J. Park, 'Boosting sodium-ion battery performance using an antimony nanoparticle self-embedded in a 3D nitrogen-doped carbon framework anode', *Chemical Engineering Journal*, vol. 429, Feb. 2022, doi: 10.1016/j.cej.2021.132359.